Hindawi
Advances in Civil Engineering
Volume 2022, Article ID 5995724, 11 pages
https://doi.org/10.1155/2022/5995724

Research Article

Mechanical Properties of the Shear Failure of Rock Masses with Prefabricated Sinusoidal Fractures

Limei Tian,[1,2] Hongzhou Zhang,[2] Wei Hong,[1] Yunxia Zhang,[2] Jinghua Zhang,[3] and Wenhui Tan[1]

[1]*School of Civil and Resource Engineering, University of Science and Technology Beijing, Beijing 100083, China*
[2]*Institute of Architectural Civil Engineering, Langfang Normal University, Langfang 065000, China*
[3]*China Petroleum Pipeline Engineering Corporation, Langfang 065000, China*

Correspondence should be addressed to Wenhui Tan; wenhui.t@ustb.edu.cn

Received 1 April 2022; Revised 15 May 2022; Accepted 27 May 2022; Published 25 June 2022

Academic Editor: Ping Xiang

A large number of sinusoidal fractures exist in the open-pit slopes of mines, and the mechanical properties of shear failure are of great significance to the stability of the open-pit slope. Sandstone specimens containing sinusoidal fractures with different undulated heights were prefabricated by the CNC sand-wire-electrode cutting technology to explore the effect of sinusoidal fractures on the mechanical properties of shear failure of rock masses. The TFD-20H/50J rock shear testing machine was used for shear tests on sinusoidal-fracture sandstone with different undulated heights. In the shear loading process, the prefabricated-fracture sandstone specimens with different undulated heights have the fracture-compacting stage, linear-elastic changing stage, bottom-up stage, and residual strength stage. Before peak strength, the sinusoidal prefabricated-fracture rock masses with different undulated heights have the precursory characteristics of decreased stress, which can provide an early warning for the instability and failure of rock masses. The undulated height of sinusoidal fractures significantly affects the fracture initiation and propagation of specimens. Fractures occur and develop from the prefabricated fractures at low undulated height (≤10 mm) to multiple ways under the high undulated height (>10 mm); that is, fractures occur at the prefabricated fractures and the end of specimens simultaneously. With the increased undulated height, the fractures expand from parallel to the slope of the prefabricated fractures to perpendicular to the prefabricated fractures. The fracture propagation direction of sinusoidal-fracture rock masses with different undulated heights is mainly from the middle of the slope surface of prefabricated fractures to the end. It is the main direction of the shear failure of sinusoidal prefabricated fractures, and the monitoring of weak planes should be strengthened in the actual slope engineering.

1. Introduction

The sloped rock masses of an open-pit mine usually have a large number of irregular structural planes, among which fractures are particularly critical to the physical and mechanical properties of rock masses. The shear-failure mechanical property of rock masses is a vital index, widely used in studying the stability of rock engineering. In slope engineering, the landslides of rock masses are usually closely related to the shear strength of slopes, with various fractures, joints, interlayers, sliding surfaces, and faults in rock masses. In the process of landslides of rock masses, the physical and mechanical properties of fractures play a crucial role in fracture initiation, expansion, and damage, and the stability of the slope is also a prerequisite for the safe production of open-pit mines. Therefore, it is vital to study the influence mechanism of fracture geometries on shear failure in fractured rock masses to explore the engineering stability of rock masses [1–3].

The material and structure of rock masses play a decisive role in the mechanical properties and law of rock-mass failure [4–8]. The common shear failure modes of rock masses along the structural plane are as follows in practical engineering: slipping damage to dam foundations [5],

Figure 1: Specimens of fractures with different undulated heights.

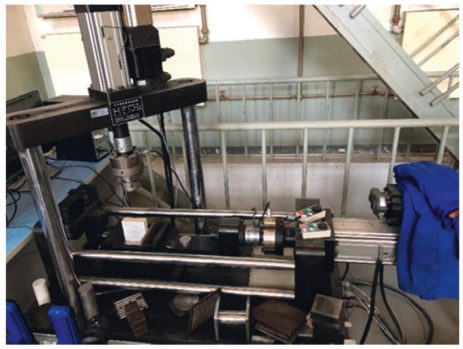

Figure 2: Shear testing machine of rocks.

unstable slipping of the sloped rock masses under low stress [6], disasters caused by static force, fault-slip earthquakes [7], and structural-plane slipped rock burst under high stress [8].

Therefore, the shear-failure mechanical properties and failure laws of structural planes of rock masses have attached great importance to rock mechanics. Scholars have studied them using indoor shear tests and numerical simulation methods [9–15]. Li et al. used cement mortar to make zigzag fractures with different undulated heights [16, 17]. Direct shear tests are performed to analyze the shear-failure mechanical properties and failure laws of zigzag fractures with different undulated heights. Zhang et al. [18] also used cement mortar to produce regular zigzag-fracture specimens with different undulated heights. The shear test studied the effects of different normal stress on the failure mechanical properties of specimens.

Foreign scholars have also studied zigzag fractures. Patton proposed a formula for calculating the shear strength of zigzag-fracture specimens [19], which has considerable limitations. Only extreme states under high/low normal stress can be investigated, and the failure of specimens cannot be well expressed under moderate normal stress. Zhang et al. used PFC^{2D} (discrete-element, particle-flow software) for numerical simulations on the specimens with different structural-plane values to analyze the strength characteristics of isotropic and heterogenic structural planes [20]. V. Sarfarazi et al. used PFC^{2D} to study the failure modes of square specimens with two horizontal fractures under the shearing action [21]. The failure modes are mainly affected by the overlap of joints, while shear strength is closely related to the failure mode.

At present, studies on irregular fractures in indoor shear tests and numerical simulations mostly consider regular zigzag fractures. A large number of sinusoidal fractures exist on the surface of the fractured rock masses of the open-pit mine slope in practical engineering, e.g., Hebei Heishan iron mine, Xigou limestone mine stope slope, and Yuebao open-pit mine. Therefore, the work prefabricated the rock masses with sinusoidal fractures and different undulated heights for shear tests. The test results have a certain reference for the safety of open-pit mines and other projects.

2. Materials and Methods

2.1. Specimen Preparation. In this test, sandstone was used as the sample material, and the geometric size of the rock masses with prefabricated fractures was $100 \times 100 \times 30$ mm. The SK7740 CNC sand-wire-cutting machine was used to prepare sinusoidal fractures, and the undulated heights of fractures were 5, 10, 15, 20, and 30 mm (see Figure 1).

2.2. Test Equipment and Loading Conditions. The TFD-20H/50J rock shear testing machine was used in the test (see Figure 2), and the normal load was first applied to specimens. The load was applied to 0.5 kN by the displacement control of 3 mm/min and then applied to 3 kN by the load control of 0.1 kN/s. Normal stress was kept stable at 3 kN, and tangential stress was loaded at a loading rate of 0.5 mm/min.

DIC equipment was used to monitor the surface deformation of specimens after pretreatment to analyze the deformation properties of specimens in the shearing process. The surface of the test piece was marked before the DIC test. First, spray a uniform layer of white primer on the side of the sample, and then spray uniform and irregularly distributed black paint speckles. A CCD camera was used to monitor the displacement changes of speckle images on the side of specimens in the shearing process. The image acquisition rate was 23 frames per second, which was used to obtain the instantaneous process of the shearing failure of specimens.

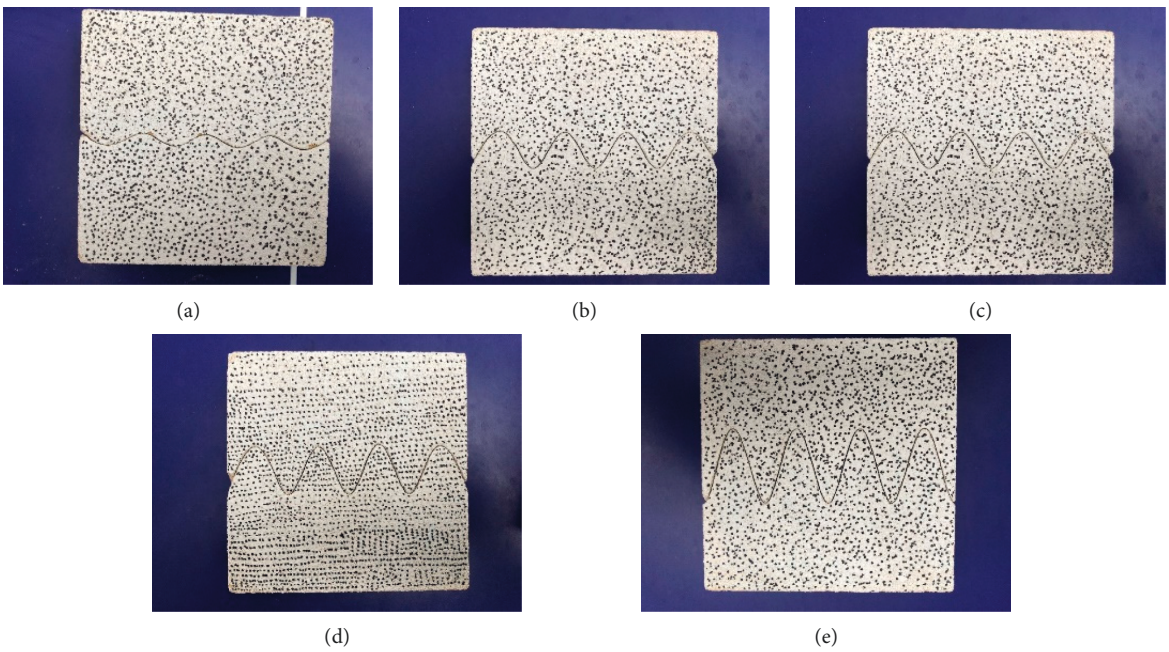

Figure 3: Specimens after marking. (a) Undulation of 5 mm. (b) Undulation of 10 mm. (c) Undulation of 15 mm. (d) Undulation of 20 mm. (e) Undulation of 30 mm.

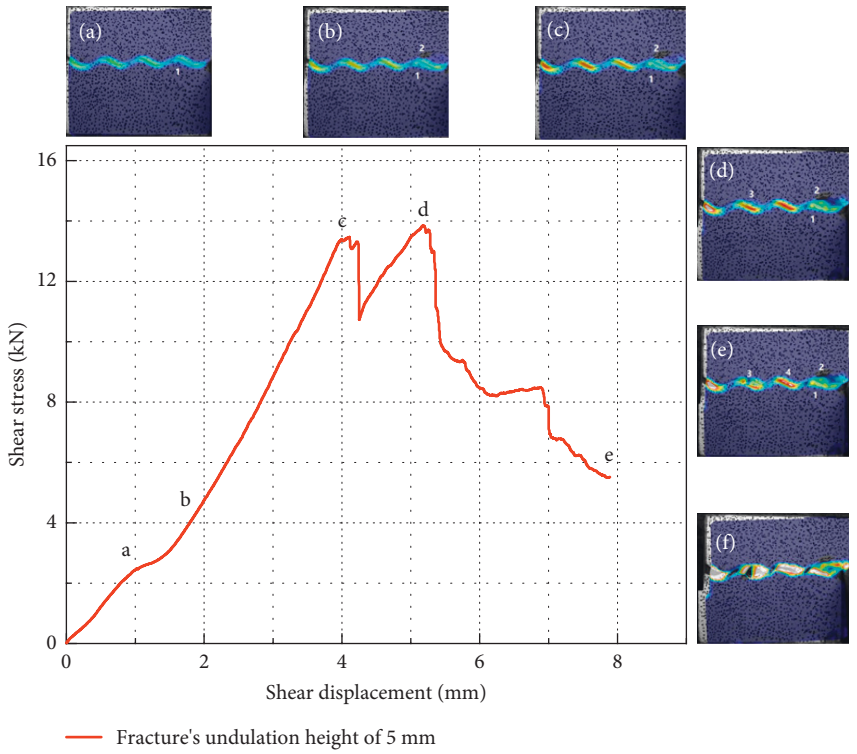

Figure 4: Shear stress-shear displacement curve of the specimen with an undulated height of 5 mm.

After the test, the monitoring images in acquisition cards were input into the computer for data processing. The monitoring range of strain could reach 0.005–2000%, which could meet the monitoring needs of shear tests. Surface-marked specimens are presented in Figure 3 for monitoring with DIC.

3. Results and Discussion

3.1. Analysis of Shear Stress-Shear Displacement Properties of Specimens under Direct Shearing. The work only analyzed the specimens with the prefabricated-fracture undulated heights of 5 and 30 mm due to the manuscript's length limit

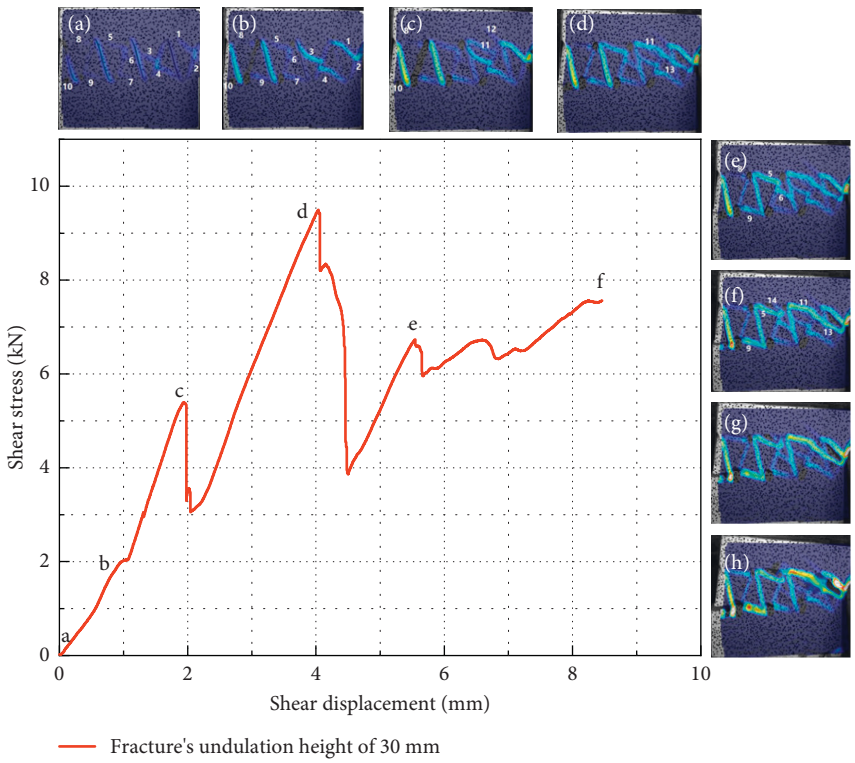

Figure 5: Shear stress-shear displacement curve of the specimen with an undulated height of 30 mm.

to analyze the shear stress-shear displacement properties of specimens under direct shearing. The details are as follows.

Figure 4 shows the shear stress-shear displacement curves of specimens with a prefabricated-fracture undulated height of 5 mm under the direct shear test as well as the development process of fractures. The characteristics of the shear stress-shear displacement curves are divided into four stages: the fracture-compacting stage, linear-elastic changing stage, bottom-up stage, and residual strength stage. The properties of each stage are as follows.

Fracture-compacting stage (ab): the shear stress-shear displacement curve is concave upward. The increment of the shear displacement decreases with increased shear stress, indicating that the prefabricated fractures of specimens and the internal fine original fractures close and compact under shear stress.

Linear-elastic changing stage (bc): the shear stress-shear strain curve presents a straight-line shape and obeys Hooke's law. With increased shear stress, fractures 1 and 2 occurred and gradually extended under stress (see Figures 4 (a) and (b)). Since the tiny fractures produced are not enough to reduce the overall shear strength of specimens, shear stress continues to increase.

Bottom-up stage (cd): this stage is characterized by the tendency of specimens' shear stress to decrease first and then increase. The stress value at point *d* is greater than that at point *c*, indicating that point *d* is the peak shear stress of specimens. That increased shear stress makes the fractures expand continuously, resulting in local damage to specimens; therefore, shear stress decreases immediately.

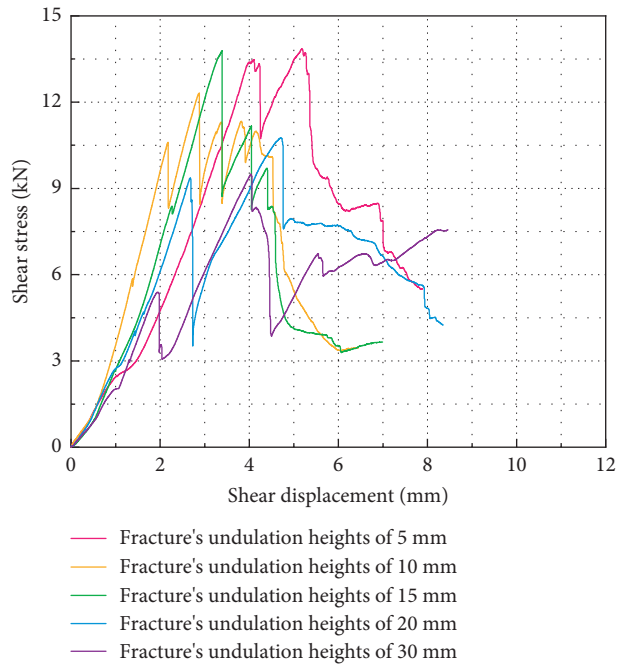

Figure 6: Shear stress-shear displacement curves of specimens with fractures having different undulated heights.

However, local damage is not enough to reduce the overall bearing capacity, and specimens still have a high bearing capacity. Thus, the shear stress of specimens continues to increase. Figure 4(e) shows new fractures that appear in specimens and develop in this process.

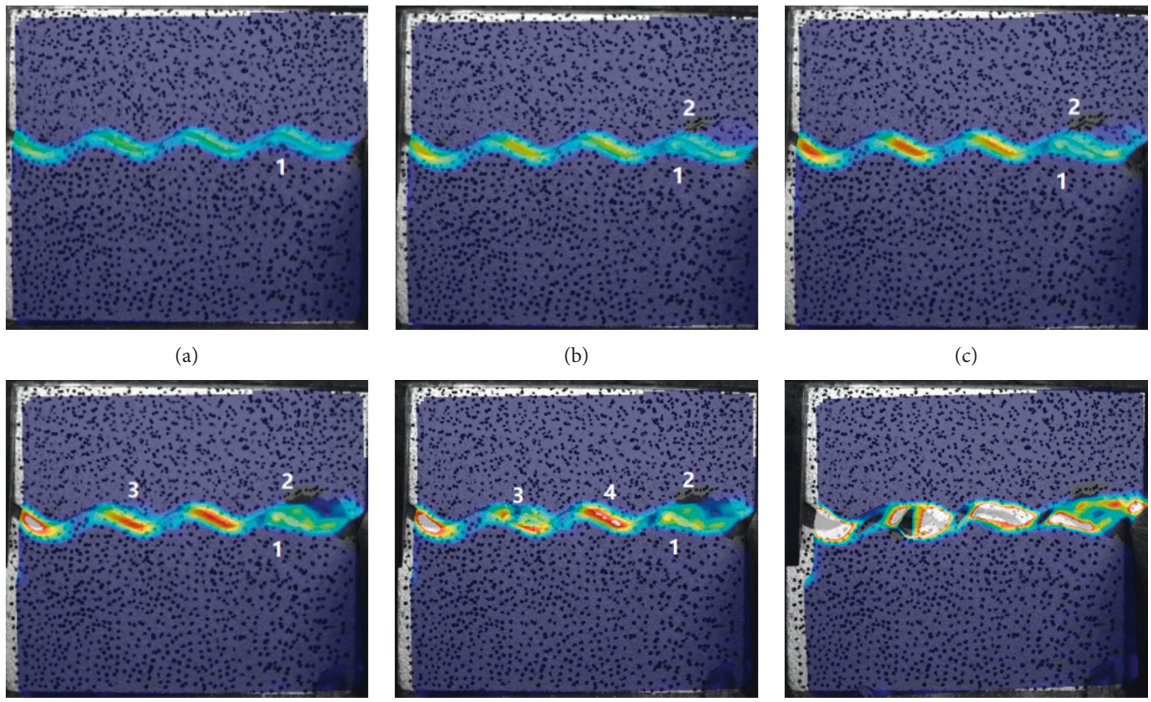

Figure 7: Failure process of the specimen with an undulated height of 5 mm under DIC monitoring.

Residual strength stage (de): fractures are further expanded under shear stress during this period. Damage occurs at the prefabricated sinusoidal fractures, causing large-scale fractures to penetrate each other and the specimens to lose most of their bearing capacity. At this time, the strength of the specimens is provided by internal friction force, and Figure 4(f) shows the final failure of the specimens.

Figure 5 shows the shear stress-shear displacement curve of the specimen with the prefabricated-fracture undulated height of 30 mm in the direct shear test as well as the development process of fractures. According to the properties of the shear stress-shear displacement curve, it is divided into five stages: the fracture-compacting stage, linear-elastic changing stage, first and second bottom-up stages, and residual strength stage.

Fracture-compacting stage (ab): the shear stress-shear displacement curve is concave upward. The increment of the shear displacement decreases with increased shear stress, indicating that the prefabricated fractures of specimens and the internal fine original fractures close and compact under shear stress.

The linear-elastic changing stage (bc): the shear stress-shear displacement curve presents a straight-line shape and obeys Hooke's law. Fractures occur and expand. In Figure 5(a), fractures 1, 2, 3, 4, and 5 occur and expand with the large undulated height due to compression of shear stress.

The 1st bottom-up stage (cd): this stage is similar to the bottom-up stage with an undulated height of 5 mm. However, the specimens with an undulated height of 30 mm rise more after the curve descends. Figure 5(c) shows that local fractures occur at the top and middle of sinusoidal fractures, which decreases the bearing capacity and descends the curve. However, the fractures are small, and no major penetration occurs. There is still a strong bearing capacity, so the curve continues to rise.

The 2nd bottom-up stage (de): this stage is different from the 1st bottom-up stage, and its bottom and up sections are located after the shear stress peak. With the further expansion and penetration of fractures, the strengthening of the squeezing action near the top of the sinusoidal fracture causes the entire part of the specimen to be damaged. As a result, the specimen is unstable, and shear failure occurs, which decreases shear stress instantaneously. However, the deformation diagram shows that the damaged specimen still has bearing capacity under the squeezing action and friction, which increases shear stress again.

The residual strength stage (ef): fractures extend and penetrate under shear stress, and the overall strength of the specimen is seriously affected and eventually destroyed. In Figures 5(f) and 5(g), fractures 9 and 10 penetrate, and so do fractures 11 and 13, which significantly affect the overall strength of the specimen, and the specimen is gradually damaged.

The shear stress-shear displacement curves of the specimens with different undulated heights (see Figure 6) are used to explore the effect of prefabricated fractures with different undulated heights on the shearing effect of the specimens. Under the shearing action, the initiation and propagation of fractures are reflected in the shear stress-shear displacement diagram, and the shear stress-shear displacement curves show that the sandstone specimens

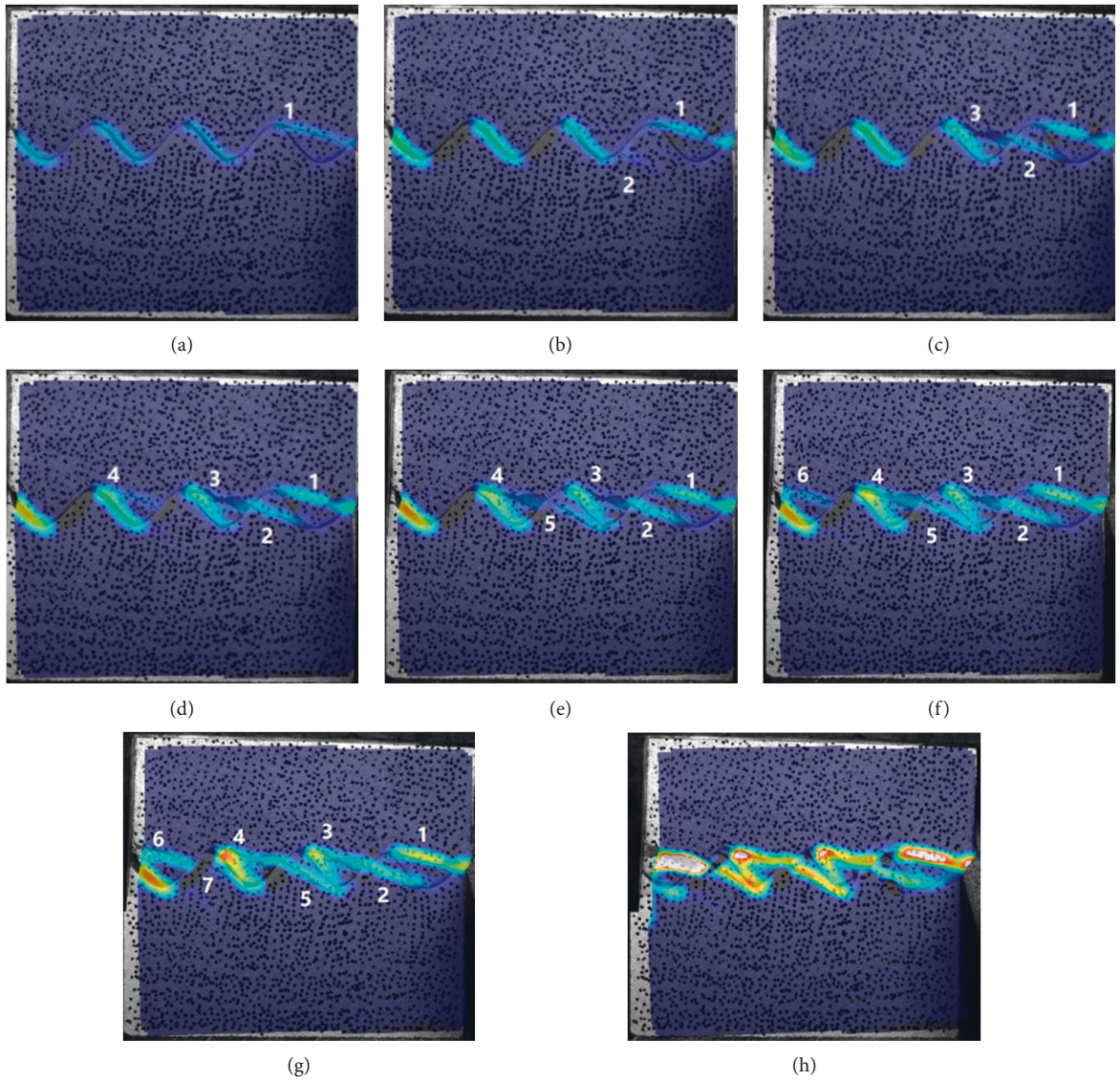

Figure 8: Failure process of the specimen with an undulated height of 10 mm under DIC monitoring.

with prefabricated fractures and different undulated heights have experienced the fracture-compacting stage, linear-elastic changing stage, bottom-up stage, and residual strength stage. At the first bottom-up stage, it rises from a relatively small stress value to peak strength. Before reaching peak strength, the rock masses with prefabricated fractures experience a brief local failure, which has few effects on the overall strength of specimens. The rock masses still have a strong bearing capacity.

The first decrease of shear stress can provide an early warning for the failure and instability characteristics of the subsequent rock masses. According to the analysis of the shear stress-shear displacement curves, shear stress does not rapidly decrease to a minimum value after the specimens reach peak strength. Instead, it goes through multiple bottom-up stages and enters a stable stage, indicating that the specimen still has certain strength after peak strength and can maintain a certain bearing capacity.

3.2. Fracture-Extension Process of Specimens in the Direct Shear Test. Figure 7 shows the fracture-expansion process of the specimen when the undulated height of the prefabricated fracture is 5 mm. Under shear stress, the fracture-development position is the stress concentration area inside the prefabricated fracture. Figure 7(a) shows that fracture 1 occurs at the bottom of the sinusoidal fracture and expands along the slope to the middle of the next sloped fracture. At the initial stage of the shear loading, the main force direction of the specimen is approximately parallel to the slope surface and prone to failure. Meanwhile, fracture 2 expands with further increased shear stress, parallel to shear stress. It eventually penetrates with the tip of the prefabricated fracture and suffers failure (see Figures 7(b) and 7(c)). The prefabricated fracture has a major influence on the fracture propagation direction of specimens.

Then fracture 3 occurs, and its position is farther from fractures 1 and 2. As stress concentration appears, fracture

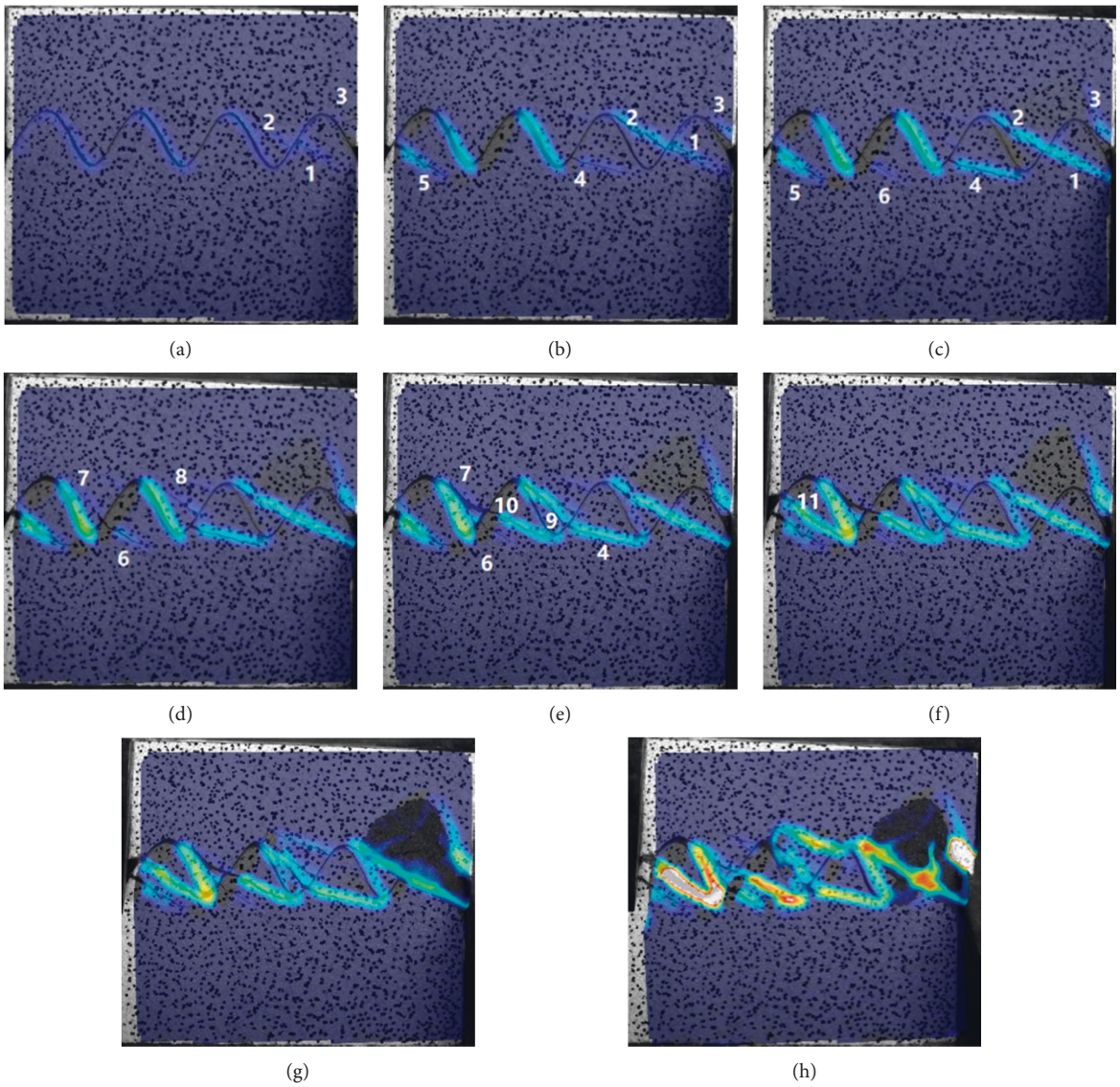

Figure 9: Failure process of the specimen with an undulated height of 15 mm under DIC monitoring.

initiation begins. Fracture 3 and prefabricated fractures penetrate with increased shear stress. Meanwhile, prefabricated fracture 4 in the connecting parts of fractures 1, 2, and 3 also occurs and expands rapidly (see Figures 7(d) and 7(e)) because fractures penetrate each other. Finally, the four fractures are fully expanded and penetrated, and the specimen suffers a shear failure. Figure 7(f) shows the final failure.

Figure 8 shows the fracture-expansion process of the specimen when the undulated height of the prefabricated fracture is 10 mm. The fracture-development location is still the stress concentration area inside the prefabricated fracture. However, compared with the specimen with an undulated height of 5 mm, there are obvious differences in stress concentration parts. The squeezing effect on the top of the prefabricated fracture is more intense and stress concentration is more obvious due to the "climbing" effect in the shearing process. Therefore, fracture 1 expands from the top of the prefabricated fracture to the end of the specimen under stress, and fracture 2 also expands (see Figures 8(a) and 8(b)). As shear stress gradually increases, fractures 3 and 4 also develop. However, Figures 8(c) and 8(d) show that fractures 3 and 4 both occur from the top of the sinusoidal fracture and expand to the middle, parallel to the wave direction of the sinusoidal fracture. Meanwhile, fracture 3 and the prefabricated fracture penetrate each other under the influence of fracture 2, so the specimen loses part of the bearing capacity. Sinusoidal fractures under the shearing action play a leading role in the development, expansion, and penetration of the fractures in the specimen.

With the action of shear stress, fracture 5 occurs from the bottom of the sinusoidal fracture and expands to the middle, which has the same expansion characteristics as fractures 3 and 4. At this point, the specimen has lost most of its bearing capacity (see Figures 8(e) and 8(f)). Finally, fractures 6 and 7

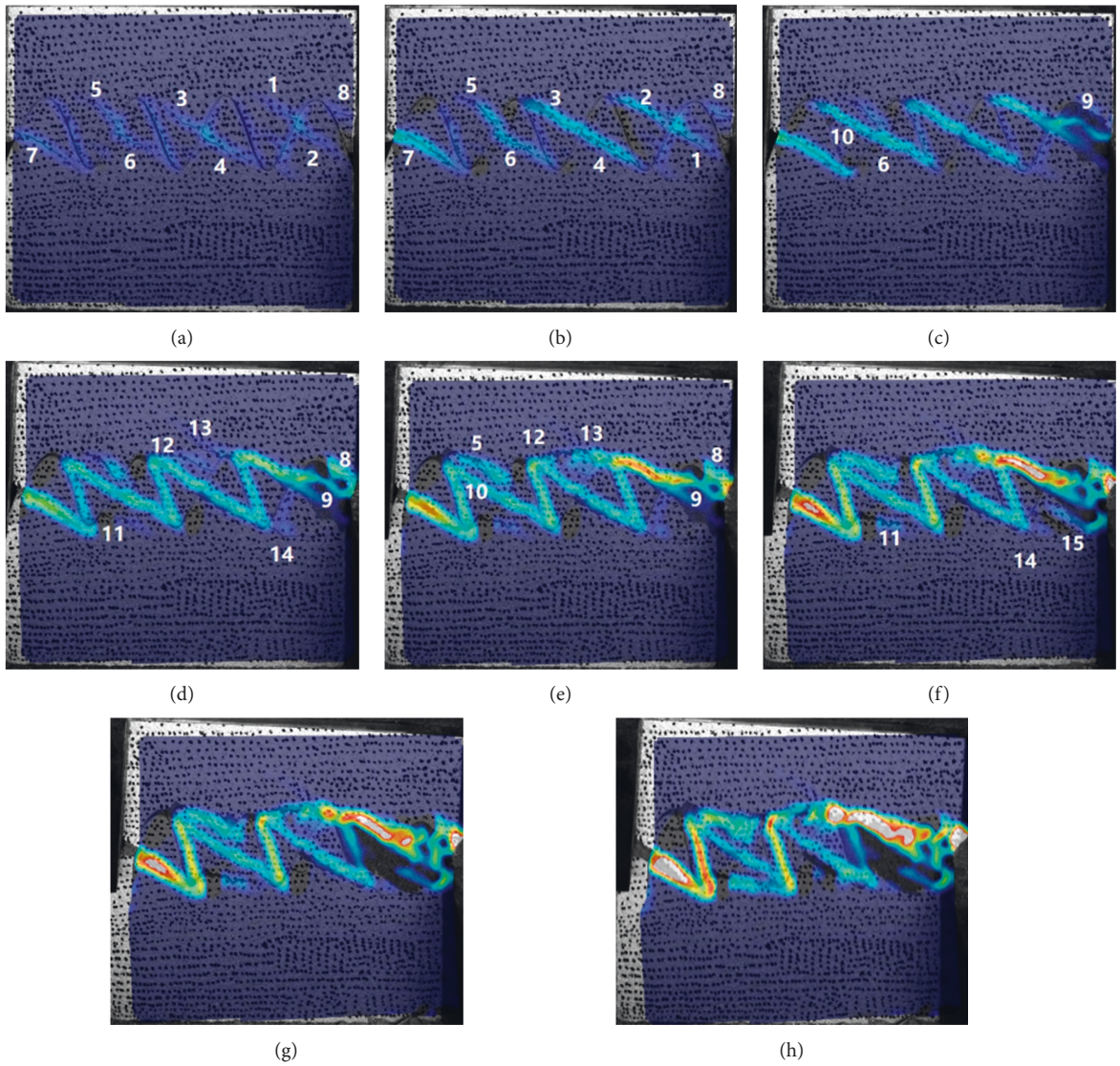

Figure 10: Failure process of the specimen with an undulated height of 20 mm under DIC monitoring.

gradually develop to the failure of the specimen in the same way (see Figures 8(g) and 8(h)).

The above fracture propagation process shows that when the undulated height of the prefabricated fracture is 10 mm, the development direction of fractures is mainly parallel to the "climbing" section of the sinusoidal fracture. It is the dominant direction of the failure of the specimen, and the monitoring of this direction should be strengthened in the actual slope engineering.

Figure 9 shows the fracture-extending process of the specimen with an undulated height of 15 mm. Fractures 1 and 2 still occur from the stress concentration zone in the middle of the sinusoidal fracture, and fracture 3 is also generated at the end of the specimen (see Figure 9(a)). With gradually increased shear stress, fractures 4, 5, and 6 expand (see Figures 9(b) and 9(c)). The above three fractures appear from the middle and lower parts of the sinusoidal fracture and develop perpendicular to the fracture, which is approximately parallel to the shearing direction. The increased undulated height of the prefabricated sinusoidal fracture changes the direction of the weak planes of rock masses. At this time, fractures 1 and 2 penetrate each other under stress, forming a penetrated fracture, which affects the bearing capacity of the specimen. After occurring from the top of the sinusoidal fracture, the fracture develops in the middle and gradually penetrates the existing fracture. Some secondary cracks also occur in the specimen. The final specimen is damaged under shear stress (see Figures 9(f)–9(h)).

Figure 10 shows the fracture-expansion process of the specimen with an undulated height of the prefabricated fracture of 20 mm. The fracture development is in the stress concentration area. Fractures occur and expand from the middle of the prefabricated fracture to the end, and some are also generated at the end of the specimen. With increased shear stress, fractures 1, 2, 3, 4, 5, 6, and 7 occur and expand from the stress concentration area inside the fracture; fracture 8 appears from the end of the specimen (see Figure 10(a)). Under shear stress, fractures 1 and 2, fractures

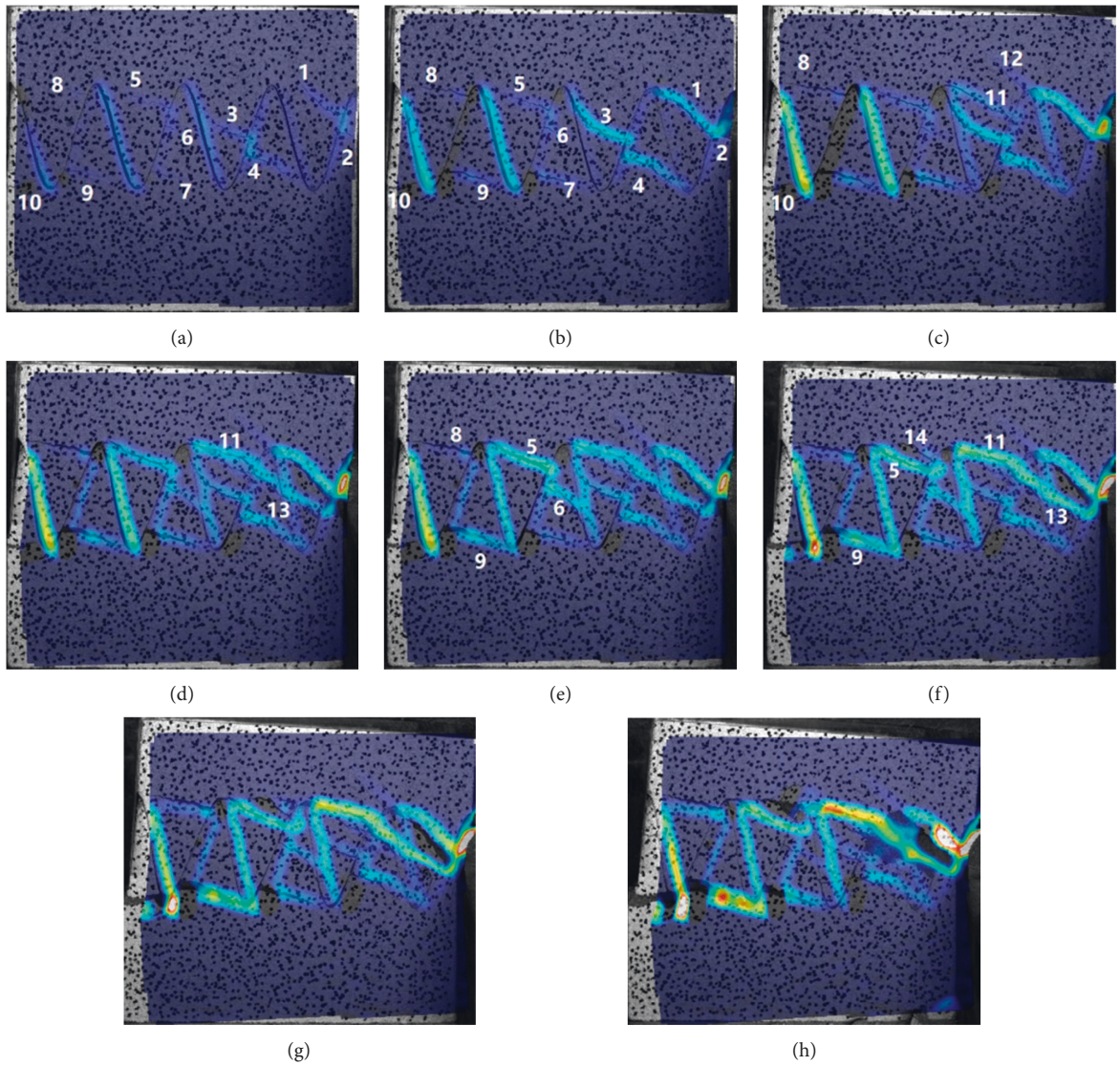

Figure 11: Failure process of the specimen with an undulated height of 30 mm under DIC monitoring.

3 and 4, and fractures 5 and 6 further expand and penetrate each other.

Fracture 7 also penetrates with the prefabricated fracture, and the strength of the specimen is affected (see Figure 10(b)). Then, the tip of the prefabricated fracture is partially destroyed, and fracture 9 occurs at the end of the specimen and penetrates with the prefabricated fracture. After arising, fracture 10 penetrates with fracture 6 under shear stress (see Figure 10(c)). Multiple fractures gradually penetrate each other under stress. Fractures 12, 13, and 14 occur and expand, and fractures 12 and 13 penetrate each other after rapid extension; fractures 5 and 10 also penetrate. At this time, the shear resistance of the specimen is greatly reduced (see Figures 10(d) and 10(e)). Finally, fracture 11 penetrates with the prefabricated fracture. The specimen generates a large number of tiny fractures, which eventually causes the failure of the specimen (see Figures 11(f)–11(h)).

Figure 11 shows the fracture-extension process of the specimen with an undulated height of the prefabricated fracture of 30 mm. The undulated height is the maximum explored in the work. Figures 11(a) and 11(b) show that the fractures occur near the end of the sinusoidal prefabricated fracture and extend to the other end. When the undulated height increases, stress concentration near the tooth tip is more obvious in the shearing process, and the bearing capacity is weak. Therefore, it causes the first fracture there. Fractures 1, 3, 4, 5, 6, 7, 8, and 9 arise from the internal stress concentration areas of the prefabricated fractures. Fractures 2 and 10 are generated at the left and right ends of the specimen, respectively, and fracture 2 quickly penetrates with the prefabricated fracture and causes partial failure of the specimen. The expanded direction of fractures is perpendicular to the prefabricated fracture (see Figures 11(a) and 11(b)).

With increased shear stress, fractures 8 and 10 gradually form the penetrated path between the end and prefabricated fracture, and fractures 11 and 12 occur and expand (see Figure 11(c)). Fracture 11 generates secondary fracture 13

and penetrates with the prefabricated fracture (see Figure 11(d)). Fractures 5 and 6, fractures 5 and 9, and fractures 11 and 13 penetrate under stress. According to the stress cloud diagram, fractures 5, 9, 11, and 13 are located in the stress concentration area. At this time, the strength of the specimen is seriously affected, and a new fracture 14 occurs (see Figures 11(e) and 11(f)). Finally, the specimen is damaged under shear stress (see Figures 11(g) and 11(h) for results).

To sum up, with the increased undulated height of prefabricated fractures, fractures expand from the stress concentration area inside the prefabricated fracture to the stress concentration area and the end of specimens. For specimens with undulated heights of 5 and 10 mm, fractures only develop from the stress concentration area inside the prefabricated fracture. For the specimens with the undulated heights of 15, 20, and 30 mm, the fracture occurs and expands from the end of the specimen except for the stress concentration area. With the increased undulated height, the fracture expands from parallel to the slope of the prefabricated fracture to perpendicular to the prefabricated fracture. For the specimen with an undulated height of 5 mm, the fracture propagation direction is parallel to the slope of the prefabricated fracture.

For those with undulation heights of 10, 15, 20, and 30 mm, the fracture-expansion direction is approximately perpendicular to the prefabricated fracture. Fractures increase with the increased undulated height. Based on DIC monitoring, specimens with the undulated heights of 5, 10, and 15 mm have 4, 7, and 11 fractures, respectively; when the undulated heights are 20 and 30 mm, there are 15 and 14 fractures, respectively. Although the undulated height of prefabricated fractures changes, fractures expand from the middle to the end of the slope surface of the prefabricated fracture. This direction is the main fracture direction in the shear failure of the sinusoidal prefabricated fracture, and the monitoring of the weak plane should be strengthened in the actual slope engineering.

4. Conclusions

Taking sandstone as the research object, the work performed the direct shear test of sinusoidal fractures with different undulated heights to study the influences of the undulated heights on the shear stress-shear displacement characteristics of the sinusoidal-fracture specimens and the fracture-evolving process. The following conclusions were obtained by the comparative analysis of the results:

(1) During the shear test, the prefabricated-fracture sandstone specimens with different undulated heights had the fracture-compacting stage, linear-elastic changing stage, bottom-up stage, and residual strength stage.

(2) Under the shearing action, the rock masses with the sinusoidal prefabricated fractures of different undulated heights had the precursory characteristics of decreased stress before peak strength. However, it had little effect on the overall strength of the specimen, so the feature could be used for early warning of instability and failure of rock masses. After the peak, the stress of the specimen appeared several times at the bottom-up stage and finally entered a stable stage, indicating that the specimen still had a certain bearing capacity after failure.

(3) The undulated height of the sinusoidal fracture significantly affected the fracture initiation and propagation of the specimen. The fracture occurred and developed from the prefabricated fracture at a low undulated height (≤10 mm) to multiple ways at a high undulated height (>10 mm); that is, the fracture occurred at the prefabricated fracture and the end of the specimen simultaneously. With the increased undulated height, the fracture expands from parallel to the slope of the prefabricated fracture to perpendicular to the prefabricated fracture.

(4) On the whole, the fracture development of rock masses of sinusoidal fractures with different undulated heights had commonalities. That is, the fracture expanded from the middle slope of the prefabricated fracture to the end, which was the main fracture direction in the shear failure of the sinusoidal prefabricated fractures. In the actual slope engineering, the monitoring of the weak plane should be strengthened.

Data Availability

The experimental data used to support the findings of this study are included within the article.

Conflicts of Interest

The authors declare that there are no conflicts of interest regarding the publication of this paper.

Acknowledgments

The work was supported by the Research and Practice Project of Higher Education Teaching Reform of Hebei Province (Grant no. 2021GJJG364), the Major Project of Langfang Normal University (Grant nos. K2018-03), the Natural Science Foundation of Hebei Province of China (Grant no. A2021408004), and Science and Technology Project of Hebei Education Department (Grant no. QN2020140).

References

[1] C. C. Xia and Z. Q. Sun, *Joint Mechanics of Engineering Rock Mass*, Tong ji University Press, Shanghai, China, 2002.

[2] H. Zhou, F. Z. Meng, and C. Q. Zhang, "Shear failure characteristics of structural plane and its application in studying slip-type rockburst," *Chinese Journal of Rock Mechanics and Engineering*, vol. 34, no. 9, pp. 1729–1738, 2015.

[3] D. Stead and A. Wolter, "A critical review of rock slope failure mechanisms: the importance of structural geology," *Journal of Structural Geology*, vol. 74, no. 5, pp. 1–23, 2015.

[4] F. Ding, X. Wu, P. Xiang, and Z. Yu, "New damage ratio strength criterion for concrete and lightweight Aggregate concrete," *ACI Structural Journal*, vol. 118, no. 6, 2021.
[5] M. R. Li, Y. Chen, and L. Zhang, "Influence and treatment of the stability of gravity dam foundation with multiple structures under complex geological conditions," *Rock and Soil Mechanics*, vol. S1, pp. 328–333, 2014.
[6] Q. Xu, D. X. Zhang, and G. Zheng, "Failure mode and stability analysis of the left bank abutment slope of jinping I hydropower station in the construction period," *Chinese Journal of Rock Mechanics and Engineering*, vol. 6, pp. 1183–1192, 2009.
[7] Y. S. Pan, L. G. Wang, and M. T. Zhang, "Theoretical and experimental research on the occurrence of fault rock burst," *Chinese Journal of Rock Mechanics and Engineering*, vol. 06, p. 642, 1998.
[8] C. Zhang, X.-T. Feng, H. Zhou, S. Qiu, and W. Wu, "Case histories of four extremely intense rockbursts in deep tunnels," *Rock Mechanics and Rock Engineering*, vol. 45, no. 3, pp. 275–288, 2012.
[9] J. L Pan, M. F Cai, P. Li, and Q.-F. Guo, "A damage constitutive model of rock-like materials containing a single crack under the action of chemical corrosion and uniaxial compression," *Journal of Central South University*, vol. 29, no. 2, pp. 486–498, 2022.
[10] Y. J. Jiang, S. H. Zhang, and H. J. Luan, "Numerical simulation of dynamic contact characteristics of rock-mass structural plane under shear loads," *Journal of China Coal Society*, vol. 47, no. 1, pp. 233–245, 2022.
[11] S. G. Du, Y. J. Lv, and Z. Y. Luo, "Combined test system and primary application of the shear strength and size effect of the rock-mass structural plane," *Chinese Journal of Rock Mechanics and Engineering*, vol. 40, no. 7, pp. 1337–1349, 2021.
[12] M. Ma, Q. Guo, J. Pan, C. Ma, and M. Cai, "Optimal support solution for a soft rock roadway based on the drucker-prager yield criteria," *Minerals*, vol. 12, no. 1, p. 1, 2021.
[13] J. Pan, F. Ren, and M. Cai, "Effect of joint density on rockburst proneness of the elastic-brittle-plastic rock mass," *Shock and Vibration*, vol. 2021, Article ID 5574325, 9 pages, 2021.
[14] L. He, Z. M. Zhao, and G. Wu, "Experimental study on the characteristics of shear weakening behaviors of rock-mass structural surface morphology," *Rock and Soil Mechanics*, vol. S2, pp. 1–11, 2020.
[15] J. Pan, X. Wu, Q. Guo, X. Xi, and M. Cai, "Uniaxial experimental study of the deformation behavior and energy evolution of conjugate jointed rock based on AE and DIC methods," *Advances in Civil Engineering*, vol. 2020, Article ID 8850250, 16 pages, 2020.
[16] H. B. Li, B. Liu, and H. P. Feng, "Study on shear deformation characteristics and failure mechanism of simulated rock joint specimens," *Rock and Soil Mechanics*, vol. 7, pp. 1741–1746, 2008.
[17] H. B. Li, H. P. Feng, and B. Liu, "Research on the strength characteristics of rock joints under different shear rates," *Chinese Journal of Rock Mechanics and Engineering*, vol. 12, pp. 2435–2440, 2006.
[18] Q. Z. Zhang, M. R. Shen, and W. Q. Ding, "Mechanical properties of the structural plane under shear," *Hydrogeology & Engineering Geology*, vol. 39, no. 2, pp. 42–47, 2012.
[19] F. D. Patton, "Multiple modes of shear failure in rock," in *Proceedings of the1st Congress of International Society of Rock Mechanics*, Lisbon, Portugal, October 1966.
[20] Y. H. Zhang, D. J. Wang, and H. M. Tang, "Research on shear strength characteristics of heterostructured planes based on the PFC2D numerical test," *Rock and Soil Mechanics*, vol. 37, no. 4, pp. 1031–1041, 2016.
[21] V. Sarfarazi, A. Ghazvinian, W. Schubert, M. Blumel, and H. R. Nejati, "Numerical simulation of the process of fracture of echelon rock joints," *Rock Mechanics and Rock Engineering*, vol. 47, no. 4, pp. 1355–1371, 2014.